RSC Advances

ROYAL SOCIETY OF CHEMISTRY

www.rsc.org/advances

Albumin Stabilized Silver Nanoparticles-Clotrimazole β-Cyclodextrin Hybrid Nanocomposite for Enriched Anti-Fungal Activity in Normal and Drug Resistant Candida Cells.

Chauhan Gaurav[1], Gupta Nikhil[1], Sehrawat Deepti[1], Sourav Kalra[2], Rath Goutam[1], Goyal K. Amit [1*]

1. **DBT Lab, Indo-Soviet Friendship College of Pharmacy, Moga, Punjab, India**

2. **Bioinformatics Centre, CSIR- Institute of Microbial Technology, Chandigarh, India.**

*** Corresponding author**

Dr. Amit K Goyal

Associate Professor and Head

Department of Pharmaceutics,

ISF College of Pharmacy, Moga, Punjab, INDIA

Email: amitkumargoyal1979@gmail.com

Mobile: + 91-9878286888

ABSTRACT

Nanotechnology unlocked distinctive platforms to move inside a hybrid therapeutic zone. Currently, nano-metal technology is the targeted field with exceptional advantages. Exceptionally small size and dominance of the surface properties such as high surface charge raised a great deal of interest. This work is designed to exploit an interesting mechanistic feature i.e. multiple therapeutic targets possessed by metal nanoparticle. In this study we selected silver nanoparticles (AgNPs), which possesses well documented anti-fungal activity and a standard antifungal molecule i.e. "clotrimazole". A hybrid of AgNPs and clotrimazole was aimed to tackle clotrimazole resistance. Clotrimazole was firstly included into β-cyclodextrin cavity to render it water soluble; subsequently the drug loaded dextrin moiety is functionalized on the surface of bovine serum albumin (BSA) stabilized silver nanoparticles using 1-Ethyl-3-(3-dimethylaminopropyl)carbodiimide / N-hydroxysulfosuccinimide (EDC/NHS) chemistry. BSA stabilisation was essential to shield the physical interaction of AgNPs with clotrimazole β-cyclodextrin complex which is otherwise experienced. Spectral and morphological characterization of the complex assures the synthesis of hybrid metal complex. Cellular toxicity assay was performed to determine the toxic nature of the hybrid. This hybrid was then evaluated for its fungicidal activity on normal and clotrimazole resistant candida cells. The toxicity and efficacy outcomes revealed a much potent profile with handy therapeutic window. Mechanistic explanations for this hybrid nature were supported by aggravated apoptotic cell percentage and reactive oxygen species production in both resistant and non-resistant cells. Cell cycle arrest studies further revealed G_2/M phase cell cycle arrest, directing towards compromised cell membrane and DNA synthesis process equivalently in clotrimazole resistant cells.

Keywords: Silver nanoparticles; clotrimazole; hybrid complex; surface functionalization; fungal resistance.

1. INTRODUCTION

Drug resistance is a relative inattentiveness of a pathogenic and non-pathogenic species towards an active molecule (1). Presently drug resistance is classified depending on the mode and conduct of exposed specie. Primary resistance (in organisms never exposed in that host to the drug of interest), secondary resistance (defined as acquired resistance, only after exposure), intrinsic resistance (resistance of all or almost all isolates of one species) and clinical resistance (therapy failure or relapse of infection, which is not evident during in-vitro study)(2-4).

Azoles (or azole derivatives) is among one of the category of antifungal drugs that inhibit the 14α lanosterol demethylase, a key enzyme in ergosterol (a most prevalent sterol in the fungal plasma membrane) biosynthesis. Some reports also suggest that they may also target fungal plasma membrane lipids and may upset methylsterol biosynthesis by interacting with an associated 3-ketosteroid reductase (5). Mechanism of azole resistance can be easily understood as it resembles just another antimicrobial resistance process viz. adaptation of the target enzyme, altered drug efflux and influx, mutation of genes encoding for target enzymes. Development of active efflux pumps with the up regulation of CDR (with almost all azoles) and MDR (two different gene families of transporters encoded in candida species; CDR genes of the ATP binding cassette super family, and the MDR genes of the major facilitators class) has been demonstrated in azole-resistance(6). Binding of azoles to the enzymatic site gets halted with alterations in ERG11 (a gene encoding for lanosterol C14a-demethylase)(7). Studies also revealed some candida species have elevated intracellular

concentration of ERG11p which leads to reduced azole susceptibility. Mutation of the ERG3 gene prevents the formation of 14α-methyl-3,6-diol from 14α-methylfecosterol after the azole exposure, which is toxic product primarily responsible for the growth arrest (8, 9). Co-existing multiple resistance mechanisms can be operative in any given fungal strain with additive effects(4). Consequently the problem of antifungal resistance in immunocompromised and high–risk patients is becoming a major concern.

Metal nanoparticles exhibit numerous fascinating properties, and it is just a matter of time until more of these assets will be exploited(10, 11). Medicine and biology, diagnostic, biomedical, engineering, catalysis, pigments, high density storage, obscurant smokes, metallurgy, nanotechnology are the areas under focus(12, 13). More specifically AgNPs have also been revealed to possess potential inhibitory activity against fungal strains(14, 15)**.** AgNPs may exert an antifungal activity by disrupting the structure of the cell membrane and inhibiting the normal budding process due to the destruction of the membrane integrity(16). Kim et al revealed in a study that 80% inhibitory concentration (IC-80) on ATCC strains of T. mentagrophytes and C. albicans ranges from 1 to 7 µg ml^{-1}(17). Many other reports also described the MICs of AgNPs from 0.4 to 3.3 µg ml^{-1} against C. albicans, C. glabrata adhered cells and biofilm and at 10 µg ml^{-1} against Trichophyton rubrum (18). The properties of nanoparticles can be altered by changing their size, surface properties and concentration especially when at the nanometer scale (15).

Inspiring from the fact that co-existing multiple resistance mechanisms may result in additive effects, we propose a multiple targeting approach to weaken or eliminate the kinetics as well as possibility of drug resistance (19, 20). Entirely different targets, if approached at the same time, may synergise the overall effect and raise the probability to disorganise the resistance machinery. With such a theme we developed a hybrid macromolecular system employing two mechanistically

different antifungal moieties with common target. Clotrimazole; an imidazole derivative with a broad spectrum of antimycotic activity, inhibiting the biosynthesis of the sterol ergostol and rendering the membrane leaky with apparent disruption of the membrane bound enzyme systems (21). On the on other hand Ag-NPs possess excellent physico-chemical properties, especially surface charge. Direct membrane disruption achieved by virtue of its surface properties and sustained release of Ag^{+} ions in local environment establish its potential in this field(14). Reports are already available highlighting its antibacterial spectrum to antibiotic resistant organisms.

According to our hypothesis, simultaneous exposure of AgNPs and clotrimazole may synergise the possible inhibition; moreover concurrent exposure may weaken the resistance machinery to work against the loaded drug of the macromolecule. In this research work we have synthesised an engineered macromolecule with nanosilver in its core and the branches of clotrimazole containing nanopockets on its surface. Silver nanoparticles (~40 nm) were initially stabilized by bovine serum albumin (BSA) and the engineered silver surface is then functionalised with clotrimazole-β-cyclodextrin (CbC) complex using ethyl(dimethylaminopropyl) carbodiimide (EDC)/N-Hydroxysuccinimide (NHS) coupling. Direct functionalization of the clotrimazole molecule alone, as well its dextrin complex was also tried, but a potential interaction was experienced. Thus, non-specific adsorption of BSA on AgNP surface by the virtue of electrostatic attraction was achieved. **Figure-1** describes the cartoon representing this macromolecular strategy.

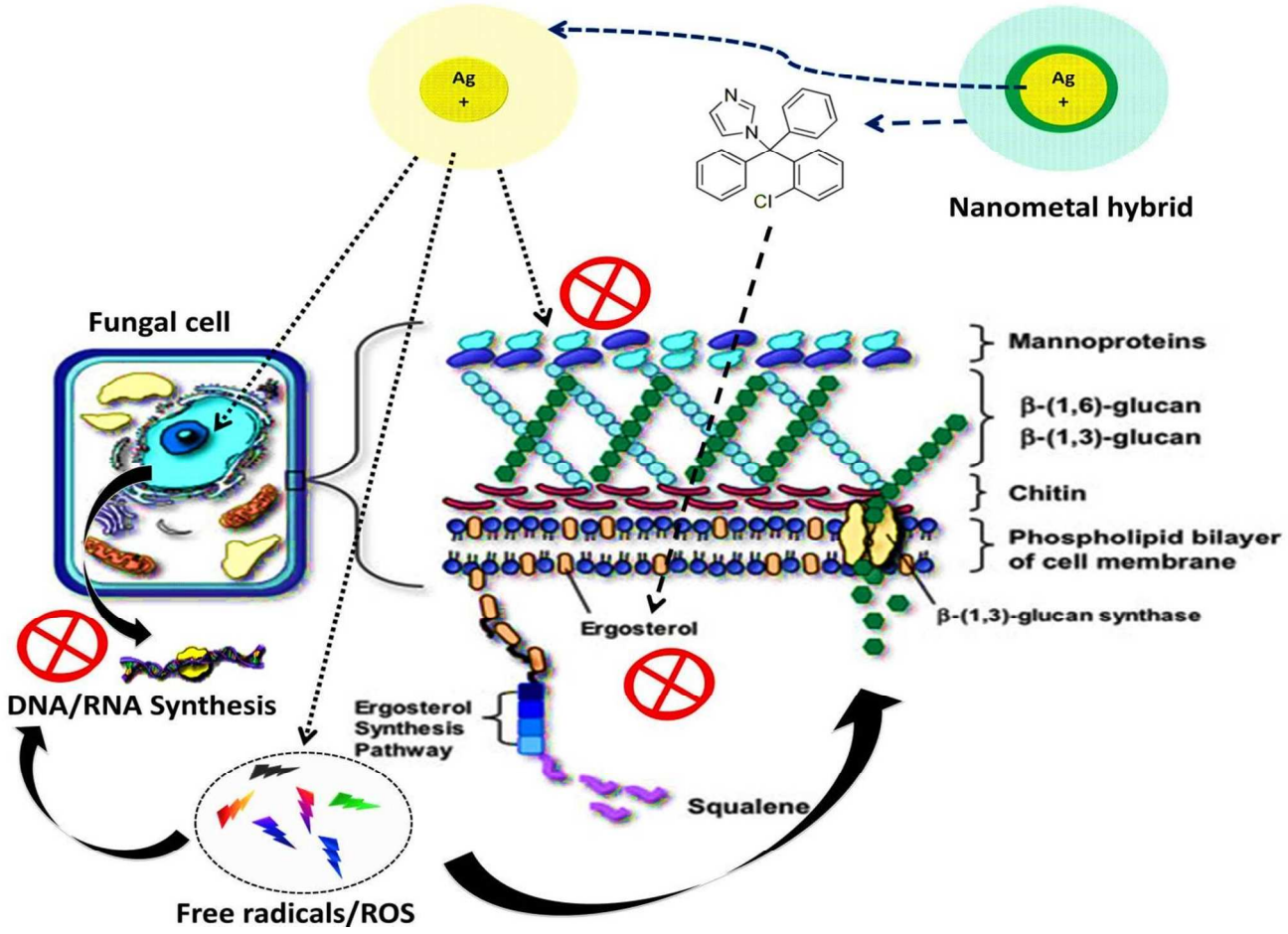

Figure-1 Macromolecular strategy using nanometal hybrid. Multiple targets of this hybrid nanocomposite, where AgNPs can cause direct damage to the fungal cell membrane, interruption of DNA replication and ATP production and generation of reactive oxygen species. Indifferently clotrimazole released from this complex provide fungal cell inhibition by inhibiting the ergosterol biosynthesis, leading to compromised fungal plasma membrane. Entirely different targets can be approached at a single time with this hybrid nanometal composite, which may improve the overall effect and the resistance development process may get disorganised.

2. MATERIAL AND METHODS

2.1 Synthesis of BSA stabilized silver nanoparticles ($_{BSA}$AGNPs) and estimation of hard BSA corona.

Sodium borohydride ($NaBH_4$) reduction method was used to synthesise AgNPs with slight modifications. Briefly, 10 ml of (1.0) mM $AgNO_3$ was reduced with 30 ml of (2.0) mM $NaBH_4$ under controlled temperature and stirring conditions (22).

19.5 ml lemon yellow coloured AgNPs nanosuspension (100µg/ml) was then incubated with 0.5 ml of 0.5 M BSA solution in double distilled water. The reaction was allowed to proceed for 2hrs at ambient temperature and the resultant bioconjugate **($_{BSA}$AGNPs)** was centrifuged for 1hr at 13000 rpm (23).

Synthesised AgNPs and $_{BSA}$AGNPs were then characterized for particle size, polydispersity index (PDI), zeta potential using (Zeta sizer, DLS 4C Beckman Coulter, Japan), UV-VIS spectroscopy using (UV-1700 spectrophotometer, Shimadzu, Japan), FTIR Spectrophotometer (Nicolet-380, Thermo, USA), X-Ray powder diffractometry using (Bruker AXS D8 Advance Diffractometer), and morphology using transmission electron microscope (TEM - Hitachi H-7500, USA) operating at 100 kV.

Flocculation experiments were performed to assure this surface conjugation (24). **$_{BSA}$AGNPs** were exposed to saline phosphate buffer (pH 7.4 and 155mM NaCl) in 1:1 volume ratio and precipitation was checked.

Hard BSA corona was estimated as the quantity of BSA forming the tight cloud around the nanometal surface. The supernatant left after centrifugation step was subjected to the quantification of unconjugated BSA. Bicinchoninic acid (BCA) assay was performed for the quantitative

estimation of free protein at 562nm on UV-Vis spectrophotometer and using equation-1 hard BSA corona was quantified.

$$\mathbf{BSA}_{\mathbf{hard\ corona}} = \mathbf{BSA}_{\mathbf{total}} - \mathbf{BSA}_{\mathbf{supernatant}} \quad \text{.....} \textit{equation}\text{-1}$$

2.2 Synthesis of clotrimazole-β-cyclodextrin (CβC) inclusion complex

Inclusion complex was prepared by solvent evaporation encapsulation method with 1:1 molar ratio of clotrimazole and β-CD (following methodology as detailed in our previous work (25). β-CD was dissolved in 20ml deionized water and clotrimazole solution in 2 ml methanol was added to β-CD solution under stirring at 800 rpm. Stirring was continued for 12 hrs with open cap. Highly water soluble clotrimazole-B-cyclodextrin complex then was separated from the supernatant after centrifugation at 1500 rpm and then recovered by lyophilizer (Alpha 1-2 LD plus, Martin Christ, Germany). Inclusion complex was characterized by FTIR Spectrophotometer (Nicolet-380, Thermo, USA), Differential scanning calorimetry (DSC- Mettler Toledo DSC 822e), scanning electron microscopy (JSM-840 SEM, Jeol, Japan). Clotrimazole loading inside β-CD cavity was assessed by methanol based extraction method.

2.3 Synthesis of Clotrimazole-B-cyclodextrin-$_{BSA}$AgNPs (CβC-$_{BSA}$AgNPs) hybrid nanocomposite.

CβC-$_{BSA}$AgNPs nanocomposite was synthesised by using EDC based crosslinking chemistry (26). Firstly the linker was attached to the surface exposed carboxylic groups of CβC and then the crosslinking was done with exposed amino groups of hard BSA corona on the nanometal surface, to achieve a stable nanobioconjugate. The synthetic scheme for the preparation of CβC-$_{BSA}$AgNPs nanobioconjugate is displayed in **figure-2.** 20mg of CβC was dissolved in 20 ml PBS buffer solution

(pH-6). Then, the solution was added into a centrifuge tube in the presence of 60 mg EDC and 20 mg NHS. After the tube was rotated constantly for 90min, 5mg $_{BSA}$AgNPs was added into the tube and again the tube was rotated overnight. Afterwards the CβC-$_{BSA}$AgNPs nanobioconjugate was purified by dialysis to remove the uncoupled CβC. Dialysis was done using the dialysis bag with 1000 molecular weight cutoff against PBS buffer (pH-7.2). Finally the hybrid was recovered by centrifugation at 2000 rpm for 10 min and was characterized for particle size, polydispersity index (PDI), morphology using transmission electron microscope (TEM-Hitachi H-7500, USA) operating at 100 kv, zeta potential using (Zeta sizer, DLS 4C Beckman Coulter, Japan), FTIR spectroscopy (Nicolet-380, Thermo, USA), UV-VIS spectroscopy using (UV-1700 spectrophotometer, Shimadzu, Japan) and X-Ray powder diffractometry using (Bruker AXS D8 advance diffractometer).

CβC-$_{BSA}$AgNPs was further evaluated for clotrimazole and Ag content per mg of the complex. For clotrimazole content 1mg of CβC-$_{BSA}$AgNPs was digested in 1ml methanol for 6 hrs. After digestion the clotrimazole content was determine by HPLC (Waters-2707, C-18 column and 2998 PDA detector with mobile phase consisting of water 0.1% Triethylamine (pH-3.2 adjusted by using Ortho-phosphoric acid): Methanol in ratio of (25:75 v/v %) with a flow rate of 1.0 ml/minute at a detection wavelength of 215nm. Ag content present in per mg complex was observed by atomic absorption spectroscopy (AAS, Shimadzu AA-7000 Atomic Absorption Spectrophotometer).

2.4 *In-vitro* release studies

Release of both clotrimazole and Ag from CβC-$_{BSA}$AgNPs was evaluated using dialysis bags (containing 5mg CβC-BSAAgNPs) in 100ml phosphate buffer saline (PBS 7.4), at 37˚C at 100rpm in a thermostatically shaking incubator (LSB- 1005RE, Daihan Labtech. Co. Ltd. Korea). 0.5ml of sample was taken from the buffer solution after time intervals 0, 1, 2, 4, 8, 16, 32, 64 hrs. Post-sampling, the volume was swapped with fresh medium to maintain the sink

conditions. Quantification of clotrimazole was done by HPLC (as per the above mentioned method), whereas quantification of the released Ag was done by atomic absorption spectroscopy (AAS, Shimadzu AA-7000 Atomic Absorption Spectrophotometer).

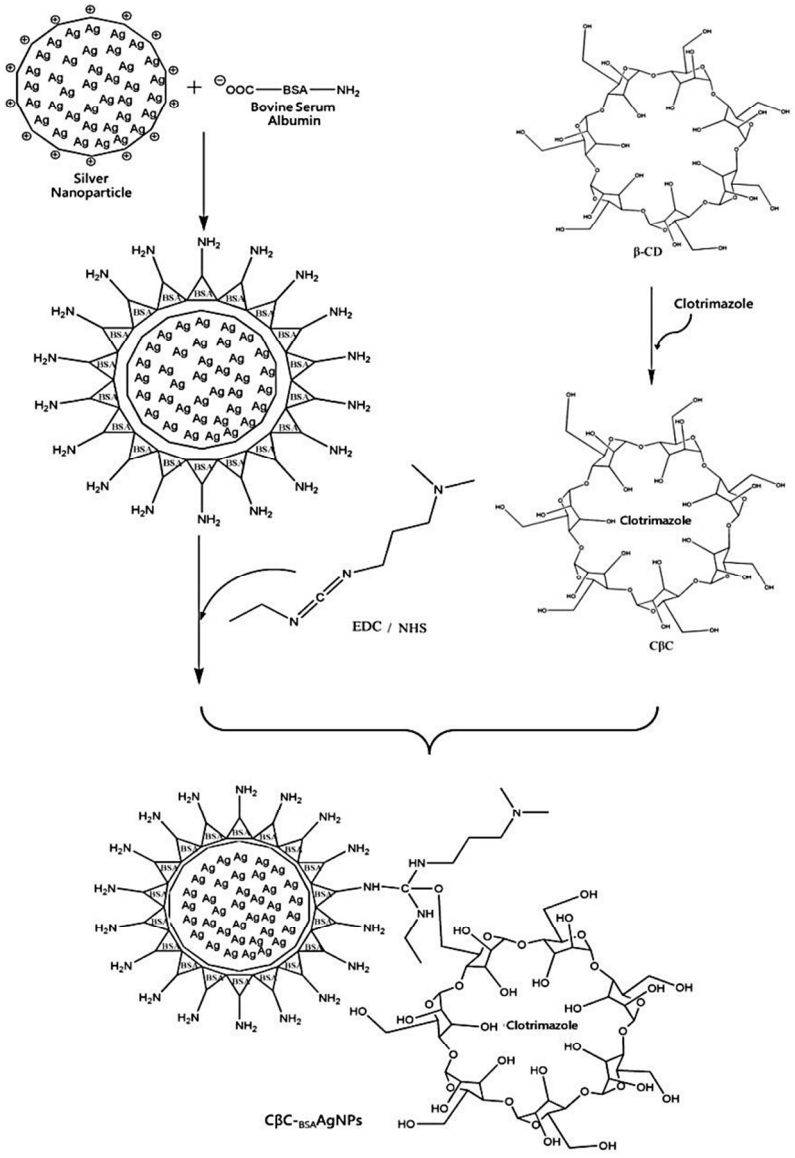

Figure-2 Synthesis scheme of albumin stabilized silver nanoparticles-clotrimazole-β-cyclodextrin (CβC-$_{BSA}$AgNPs) hybrid nanocomposite.

2.5 Cell cytotoxicity study (MTS assay)

The (3-(4,5-dimethylthiazol-2-yl)-5-(3-carboxymethoxyphenyl)-2-(4-sulfophenyl)-2H-tetrazolium) dye reduction assay in the presence of phenazinemethosulfate (PMS), produces a formazan product that has an absorbance maximum at 490-500nm in phosphate-buffered saline (27). The MTS assay was performed to determine the cytotoxic potential of CβC, AgNPs, $_{BSA}$AgNPs and CβC-$_{BSA}$AgNPs on different cell cultures. Cell viability assay was performed on Hela (Cervical cells), HEL (Human embryonic lung), VERO, and MDCK (Madin Darby canine kidney cell) cultures (28). Minimum cytotoxic concentration (MCC) i.e. the concentration required to cause a microscopically detectable alteration of normal cell morphology and Cell cytotoxicity 50% (CC_{50}) i.e. the concentration causing 50% cell death were examined from this study (29).

2.6 Antifungal susceptibility testing

2.6.1 Test organisms and test medium

C. albicans (Microbial Type Culture Collection "MTCC-183") and *C. tropicalis* (MTCC-184) strains were used in this study. The strains were inoculated onto sabouraud dextrose agar plates and incubated at 35 °C for 24 h. They were subcultured on the same medium for a further 24 hrs at 35 °C. The fungal inoculay were prepared by diluting the overnight culture with 0.9% NaCl to 1×10^6 CFU/ml. The suspensions were then further diluted in test medium i.e. RPMI-1640 (with L-glutamine, without sodium bicarbonate) supplemented with 0.165M morpholinepropanesulfonic acid (MOPS) to a final count ranging 0.5×10^3 CFU/ml. The experiments are done as per the recommendation made by NCCLS standards(30).

2.6.2 Minimum inhibitory concentration (MIC) and Inhibitory concentration 50% (IC_{50})

The antifungal effectiveness was determined against the final cell concentration of 10^6 CFU/mL for both *C. albicans* and *C. tropicalis cells*. Fungal inoculas (100µl) were added to each well of a sterile, 96-well flat bottomed microtiter plate. Arithmetic concentrations (in 100µl volume) of clotrimazole, CβC, AgNPs, $_{BSA}$AgNPs and CβC-$_{BSA}$AgNPs (ranging from 2-60µg/ml) were added systematically in the well. Each concentration was tested in triplicate for each fungal strain. 300µl of deionized sterile water were added on the exterior perimeter wells of the microplates to minimize the evaporation of the culture medium of the test wells during the incubation. For each strain two wells containing fungal suspension with no drug (growth control) and two wells containing only media (background control) were included in this plate. Optical density (OD) was measured for 24hrs at 35 °C using a microplate reader (Bio-Rad) at 405 nm and were automatically recorded every 3hrs for each well. Turbidimetric growth curves were obtained depending on the changes in the OD of fungal growth for each drug concentration and the drug-free growth control. MIC and IC_{50} values were calculated for each treatment using the same plots; the growth percentage for each drug concentration was calculated using equation-3. OD measurement were reported only after the subtraction of background ODs (ODs of fungal cells free wells). Death kinetic curves were also plotted, by challenging the fungal cells by estimated IC_{50} values of clotrimazole, CβC, AgNPs, $_{BSA}$AgNPs and CβC-$_{BSA}$AgNPs using similar OD measurement spectral method. Slopes observed in these graphs were related to the potency of the treatment.

Growth % = [(OD $_{405}$ of wells containing the test / OD_{405} of the drug free well) × 100]

…… *Equation-3.*

2.6.3 Development of clotrimazole resistance and Antifungal susceptibility testing

Cell suspension of both the candida species (0.5×10^6 CFU/ml) was exposed to their respective clotrimazole IC_{10} (concentration inhibiting 10% fungal cells). After 24 hrs of exposure both the fungal cell suspensions were individually subcultured on sabouraud dextrose agar plates at 35 °C for 24 h. After that passaged fungal cells were recovered by diluting the overnight culture with 0.9% NaCl. This experiment was repeated sequentially by exposing passaged cells with clotrimazole $IC_{20,}$ $IC_{30,}$ IC_{40} and $IC_{50.}$ Clotrimazole resistant fungal cells obtained after the gradient exposure of clotrimazole to its pre-calculated IC_{50} were again tested for their modified MIC , IC_{50} and death kinetics against clotrimazole, CβC, AgNPs, $_{BSA}$AgNPs and CβC-$_{BSA}$AgNPs using microdilution assay (as done previously).

2.7 Estimation of early apoptosis and reactive oxygen species (ROS) production

2.7.1 Annexin V–propidium iodide double staining Apoptotic changes

The early stages of apoptotic phenomenon in the treated fungal cells can be detected with fluorescein isothiocyanate (FITC)–Annexin V staining (to study the expression of phosphatidylserine on apoptotic fungal cells) and propidium iodide (to study the compromised membrane permeability of treated cells) based double-staining method. Non-resistant and resistant fungal cells were digested for 1 h at 28 ºC in a potassium phosphate buffer (pH 6.0) containing 20 mg/ml lysing enzyme and 1M sorbitol. Protoplasts of non-resistant and resistant strains were stained with FITC-labelled Annexin V and PI using the FITC–Annexin V apoptosis detection kit (Sigma Aldrich, USA) according to the staining kit protocol. Protoplasts were incubated with MIC concentrations of clotrimazole, CβC, AgNPs, $_{BSA}$AgNPs and CβC-$_{BSA}$AgNPs and incubated for 20 min in an Annexin-binding buffer containing 5 µL FITC–Annexin V/ml and PI. Protoplasts were then examined by a flow cytometer (Becton Dickinson "BD" Accuri C6).

2.7.2 Reactive oxygen species (ROS) production

With the similar treatment protocol (as followed for apoptosis detection), treated fungal cells were incubated for 10 minutes with 5mg/ml dihydrorhodamine 123 (DHR-123). DHR-123 is oxidized by intracellular ROS to the fluorescent chromophore rhodamine 123. Samples were quantitatively analysed for the generated ROS species by flow cytometry (BD Accuri C6).

2.8 Cell cycle arrest after CβC-$_{BSA}$AgNPs treatment

Non-resistant and resistant fungal cells (in their log-phased with concentration around 1 x 10^8 cells), cultured in a yeast extract-peptone-dextrose (YPD) medium, were harvested and treated with IC_{50} concentration of CβC-$_{BSA}$AgNPs. After 6 hrs of incubation, the cells were washed with PBS and fixed with 70% ethanol overnight at 4 ºC. All the cells were treated with 200 µg/ml of RNase A and the mixture was left to react for 2 hrs at 37 ºC. For DNA staining, 50 µg/ml of propidium iodide (PI) were added and incubated for 1 hr at 4 ºC in the dark. Flow cytometric analysis was performed by (BD Accuri C6). The values represent the average of the measurements conducted in triplicate of three independent assays.

2.9 Statistical analysis

All the observations were based on 3 independent experiments. Data were expressed as mean±SEM or percentage. The results were analyzed by 1-way analysis of variance (ANOVA), and chi-square test, as applicable.

3. RESULTS AND DISCUSSION

3.1 Surface biocongucation of AgNP with BSA ($_{BSA}$AgNPs)

AgNPs were successfully synthesized with an average size of 37.5±1.3nm and a narrow PDI value of 0.254±0.37. Incubation with BSA leads to the surface coating of AgNPs resulting in increased average size to 54.2±2.8nm and PDI value of 0.291±0.19. Zeta potential value of -2.04±0.01mv indicated the inherent colloidal instability of synthesised AgNPs nanoparticles but BSA stabilization leads to a drastic change in surface potential to -18.6±0.07mv. The altered value of surface potential provides a strong conformation of improved colloidal stability of $_{BSA}$AgNPs. Characteristic absorption maxima at 416nm and a solo transverse peak indicated the nano-size and isotropic nature of the AgNPs. After BSA stabilization SPR observed a shift to 432nm with compromised intensity, this significant bathochromic and hypochromic shift resulted due to protein lead quenching of silver colloid's SPR. Comparison of FTIR spectra's revealed no significant shift in the AgNPs peaks after stabilization, and the presence of the characteristic peaks of BSA in the $_{BSA}$AgNPs spectra suggested the BSA corona formation on the hydrophobic AgNPs surface by virtue of physical interactions. X-ray diffraction (XRD) patterns of AgNPs showed sharp and intense peaks corresponding to the crystalline nature of metallic nanoparticles. Surface stabilized AgNPs showed no alteration in crystalline XRD pattern, additionally a broad amorphous BSA peak was observed at shorter 2θ range. Transmission electron microscope (TEM) revealed that synthesised AgNPs were well dispersed showing a confined distribution with particles ranging from 20-50nm (25-40 nm size dominating the population). Comparatively, TEM analysis of $_{BSA}$AgNPs revealed an obvious increase in particle size where the dominating nanoparticle population lies between 45-70nm. **Figure-3** represents the characterization report of synthesised AgNPs and surface biocongucated $_{BSA}$AgNPs.

Harsh conditions of pH, ionic strength, temperature as well as physical incompatibility with drug molecules lead to the destabilization of the nanosilver colloids. Establishing the protein corona, probably because of ionic or electrostatic and hydrophobic interactions provides a physical shield preventing the direct interaction with the silver core (24). Flocculation experiment confirmed no precipitation of $_{BSA}$AgNPs in harsh conditions presented by saline phosphate buffer, presenting a straightforward protective effect of protein cloud on metal colloid stability. Further these proteins results in the development of two kinds of protein clouds around the nanometal surface viz. hard corona (essential to prevent colloid destabilization) and second is weak/soft/loose corona (hanging or accompanied protein molecules which for a secondary layer and are not necessary for stabilization process) (31). BCA assay performed for the quantitative estimation of hard protein corona revealed the supernatant BSA concentration of 41mM/ml. Estimated free BSA amount in the supernatant was around 0.083 M and thus BSA amount in hard protein corona was calculated around 0.417 M. Studies had also shown that the corona BSA protein retains its secondary structure and the helicity to a quite good extent on the nanoparticles surface. Also some studies explored the variables for this BSA functionalization and came out with a significant decrease in the BSA quantity immobilized on the AgNPs surface with the increase in AgNPs size. Its explanation was related to the relation of surface curvature (inversely proportional to the size) of the nanoparticles and the consequent energetics involved in protein adsorption and crowding. It was also suggested that the interaction of BSA and AgNPs is majorly governed by increased changes in protein conformation and to lesser extent hydrophobic interactions.

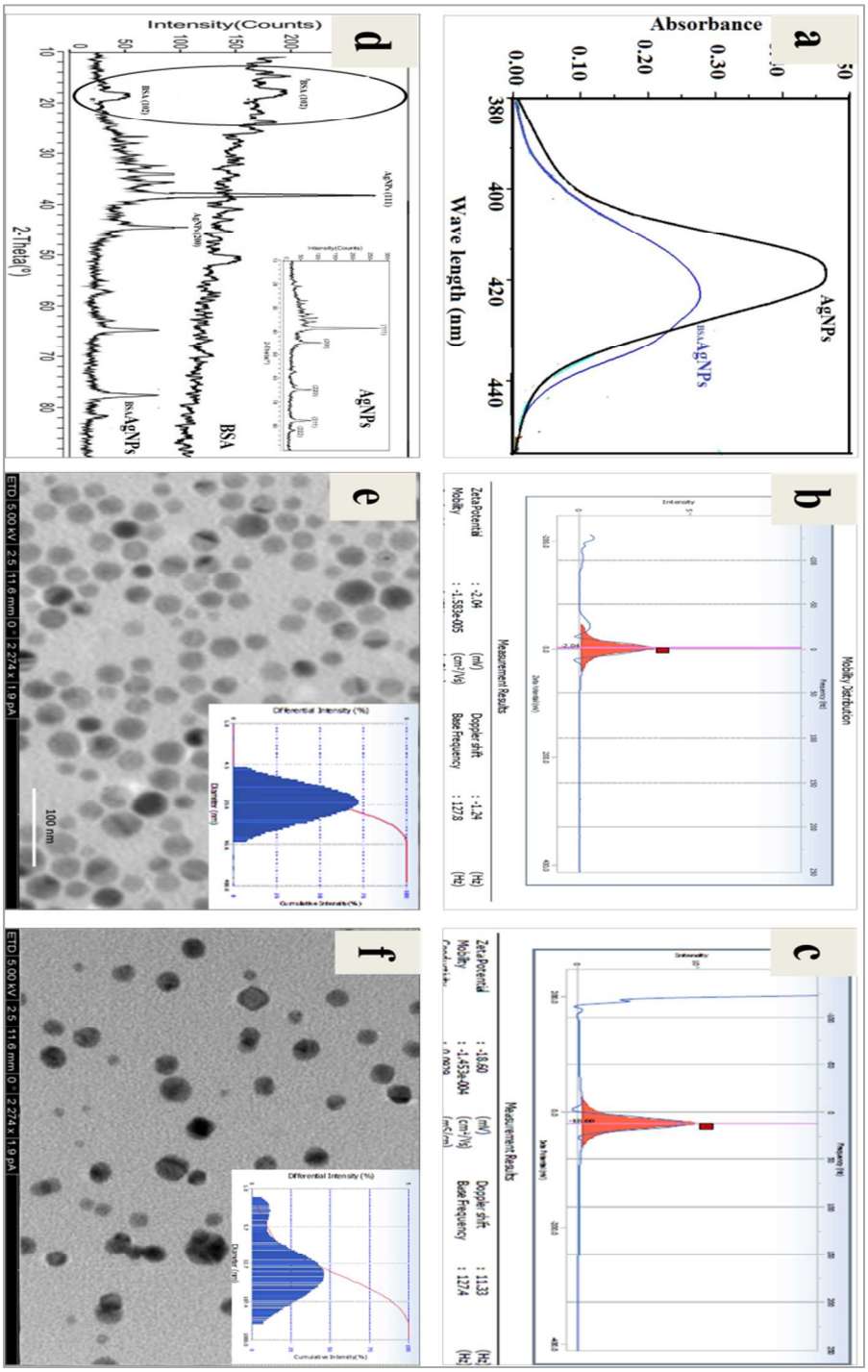

Figure-3 Characterization parameters of AgNPs and BSA stabilized AgNPs. a) UV-visible spectral comparison, b) zeta potential (AgNPs), c) Zeta potential ($_{BSA}$AgNPs), d) XRD spectral comparison, e) TEM (AgNPs), f) TEM ($_{BSA}$AgNPs).

3.2 Synthesis of clotrimazole-β-cyclodextrin (CβC) inclusion complex

CβC inclusion complex have dull white and fluffy appearance, pointing toward its amorphous nature. Aqueous saturation solubility of the complex at ambient conditions was found to be around 27.5±2.1mg/ml and the clotrimazole loading in the complex was obtained to be 84.5±4.7µg/mg. IR (KBr)cm^{-1} spectra revealed the major existence of β-CD specific peaks with a slight shift to higher/lower wave numbers while very few characteristic peaks of clotrimazole (at shorter wavelength) were observed. This indicated a successful inclusion of clotrimazole in the hydrophobic β-CD cavities. DSC thermograms of CβC complexes showed a substantial reduced intensity and broad thermodynamic peak with a shift to lower temperature (142º to 82°C) in comparison to sharp melting point of clotrimazole and β-CD. These endotherms indicate the substantial inclusion of clotrimazole in the (β-CD) cavities. Scanning electron microscopy clearly justifies the above observation of having a highly amorphous nature of clotrimazole inclusion complex. **Figure-4** displays the FT-IR, DSC and SEM characterisation of the inclusion complex. Further, drug loading study using methanol extraction method showed that lyophilized CβC complex have a significant clotrimazole loading of 68.4±3.2µg per mg of complex.

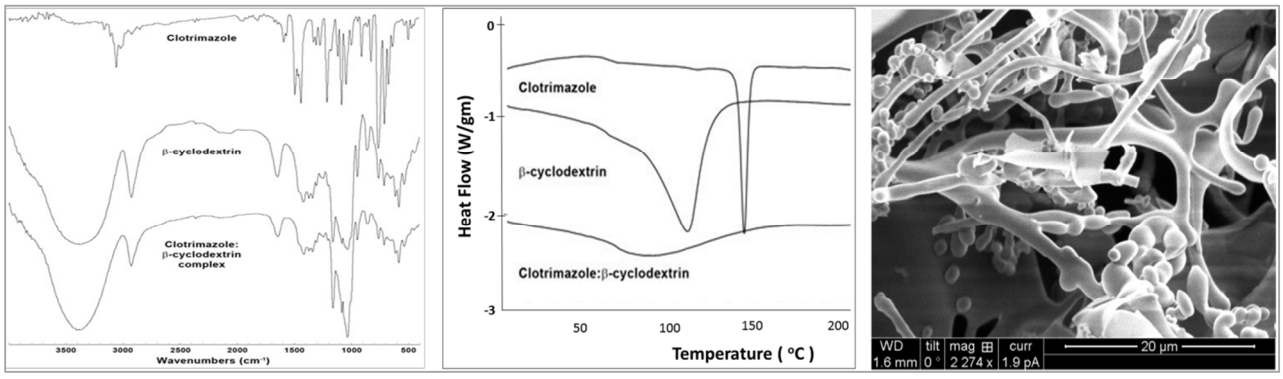

Figure-4 FT-IR, DSC and SEM image of clotrimazole-β-cyclodextrin (CβC) inclusion complex.

3.3 Synthesis of clotrimazole-β-cyclodextrin-$_{BSA}$AgNPs (CβC-$_{BSA}$AgNPs) hybrid nanocomposite.

CβC-$_{BSA}$AgNPs nanocomposite was synthesised as per the above mentioned procedure. Conjugation of CβC to BSA coating of AgNPs was obtained by carbodiimide coupling. Surface exposed carboxylic group of CβC reacted with EDC to form unstable reactive ester and further addition of NHS resulted in the formation of semi-stable amine-reactive NHS-ester. Afterwards, addition of $_{BSA}$AgNPs containing amino group on the exposed protein corona of AgNPs, leads to the formation of CβC-$_{BSA}$AgNPs conjugate by a stable amide bond.

Zeta size reports revealed an increased hydrodynamic size (68.5±1.9 nm) with uniform distribution pattern (PDI-0.274±0.13) due to the surface conjugation. To confirm this surface attachment of CβC on the $_{BSA}$AgNPs surface, changes in surface potential values were observed. Considerable change in zeta potential to -22.0±0.3mv revealed the successful surface conjugation of CβC on the surface of $_{BSA}$AgNPs. TEM images revealed the increased particle size, but nanoparticles possessed compromised surface smoothness. The CβC-$_{BSA}$AgNPs conjugates was further investigated by infrared spectroscopy where FT-IR spectra showed the characteristic peaks at 1627 cm^{-1} and 1506 cm^{-1} as a result of newly formed amide bond. UV-visible spectroscopy further revelled no sharp peak, rather a wide hump corresponding to the AgNP's surface plasmon resonance was observed in the range of 425-450nm. X-ray diffraction (XRD) patterns of synthesised conjugates suggest the presence of both $_{BSA}$AgNPs and cyclodextrin peaks but with compromised intensity. Characterization parameters synthesised CβC-$_{BSA}$AgNPs nanobioconjugate are mentioned in **figure-5**. Further quantitative analysis revealed that per mg of CβC-$_{BSA}$AgNPs complex is loaded with of 572.6±4.7 µg of silver content and 83.4±1.9 µg of clotrimazole.

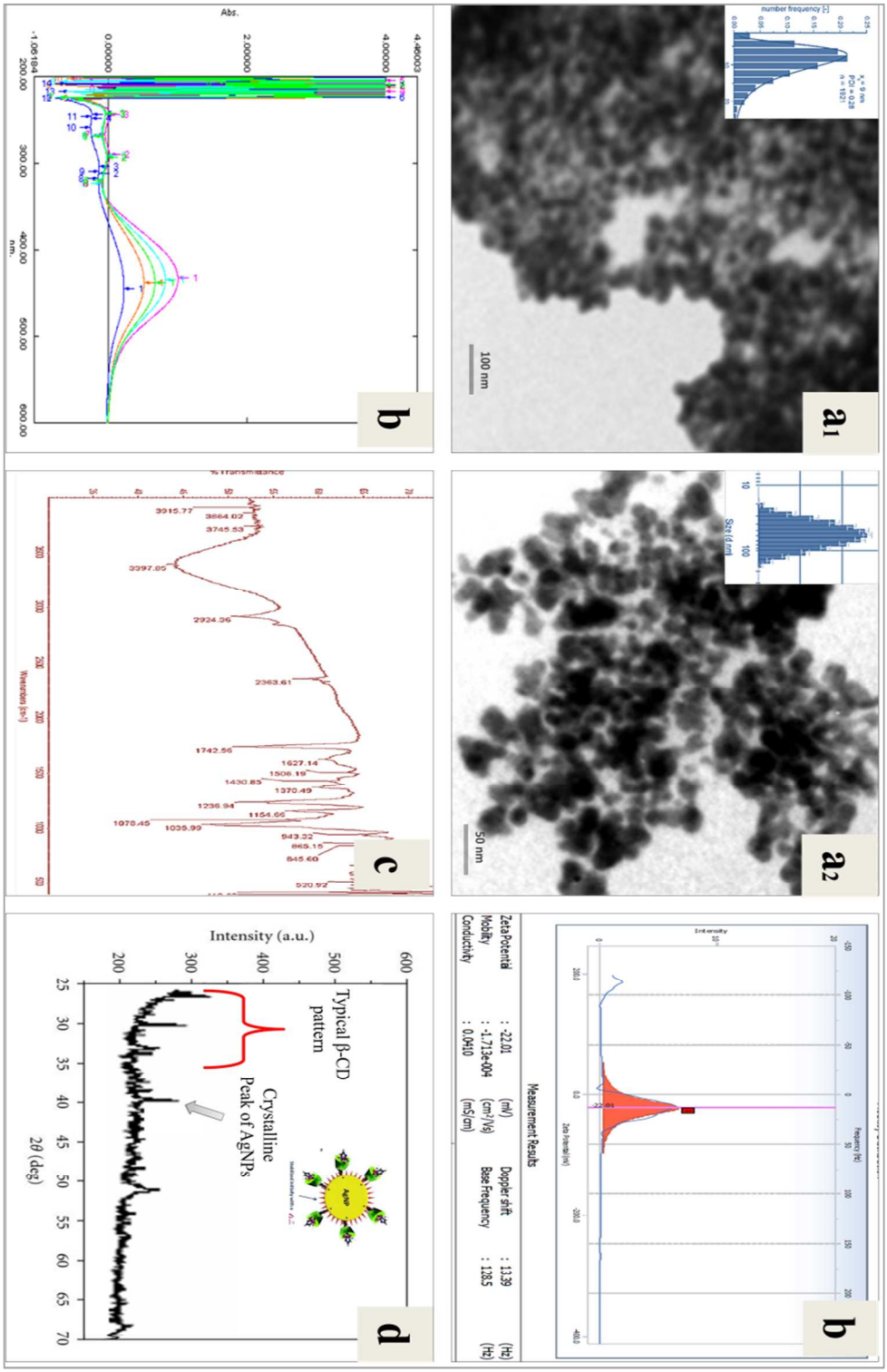

Figure-5 Characterization parameters of AgNPs and BSA stabilized AgNPs. a) UV-visible spectral comparison, b) Zeta potential (AgNPs), c) Zeta potential ($_{BSA}$AgNPs), d) XRD spectral comparison, e) TEM (AgNPs), f) TEM ($_{BSA}$AgNPs).

3.4 *In vitro* release studies

In-vitro release showed a controlled release profile for both clotrimazole and Ag from the synthesised CβC-$_{BSA}$AgNPs nanobiocomposite. Clotrimazole release followed a first order pattern initial for 16 hrs, afterwards pseudo-zero order behaviour was observed. This can be attributed to the initial ease of clotrimazole release from the edges of the cyclodextrin cavities, and in later part it become comparatively difficult to elute from the centre of hydrophobic cavity. On the other hand a sustained release pattern of silver (Ag) ions was analysed from the atomic absorption spectroscopy. AgNPs dissolution can be better understood as the ionisation of $Ag^{(0)}$ to $Ag^{(+)}$ and literature showed several relationships between the $Ag^{(+)}$ release and AgNPs size (32). Possible reasons for this kind of Ag release could be the multiple mechanistic aspects responsible for its release from the nanosilver core of the conjugate system. Among several mechanisms provided for the ionic release of silver ions, results revealed an intial and dominant desorption of the chemisorbed silver ions from the $_{BSA}$AgNPs surface (33). Moreover the presence of clotrimazole in the release environment further played its part (quite understood from the silver and clotrimazole interaction mentioned in the introductory part). Oxidative dissolution could be another simultaneous reason providing an instant release of silver ions. After 64 hrs, cumulative release observed for clotrimazole was 91.4±3.2% while for Ag ions it was 39.8±4.6%. **Figure-6** describes the release pattern followed by clotrimazole and Ag ions from the synthesised CβC-$_{BSA}$AgNPs nanobiocomposite.

In order to completely understand the kinetics of clotrimazole and ionic silver release different kinetic models were applied including zero order, first order and higuchi. On the basis of regression coefficient (R^2) from these curves it was concluded that release pattern of clotrimazole fits first order profile more closely as discussed above. In the case of Ag ions the

release had a better fit in higuchi model, which can be explained as the continuous eroding of silver ions from the nanosilver matrix of AgNPs.

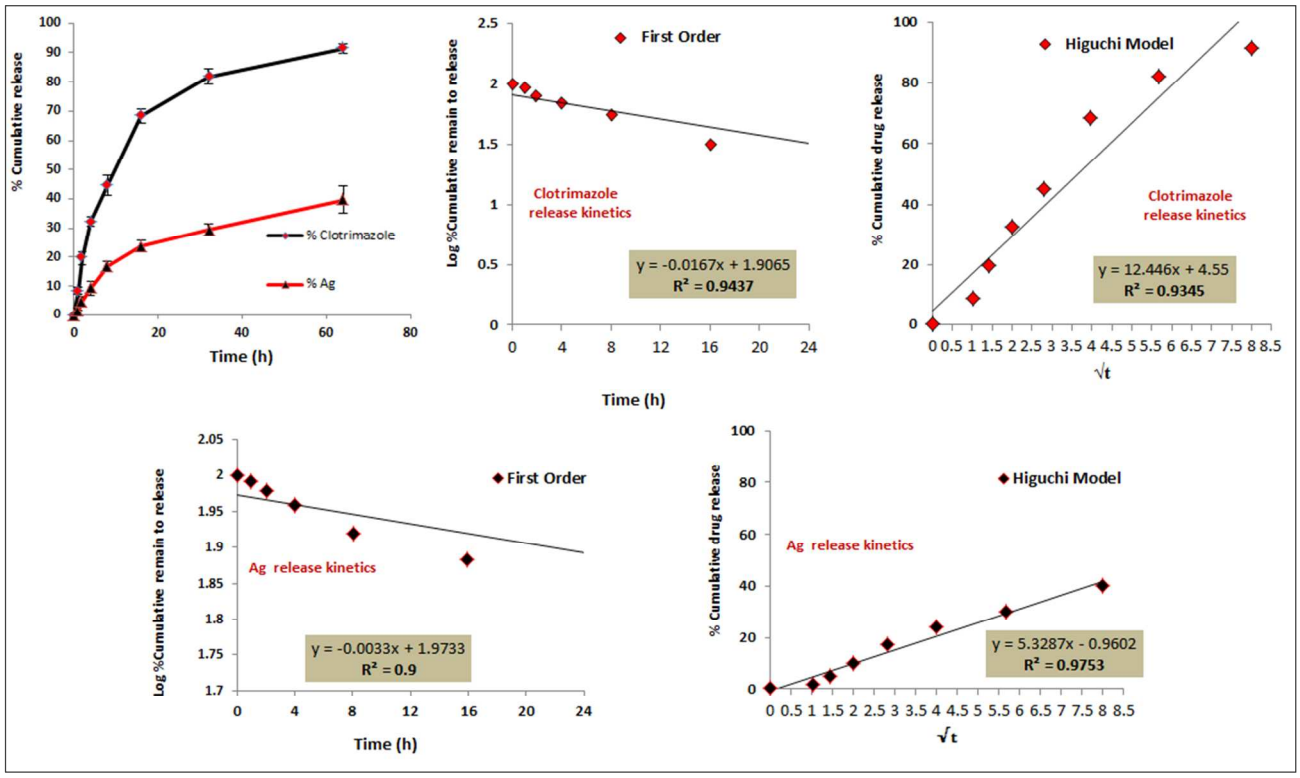

Figure-6 In-vitro release pattern of clotrimazole and Ag from the synthesised CβC-$_{BSA}$AgNPs nanobiocomposite.

3.5 Cell Viability Assay

AgNPs showed their inherent toxicity with comparatively lower MCC and CC_{50} values than, $_{BSA}$AgNPs, CβC and CβC-$_{BSA}$AgNPs as mentioned in **table-1**. CβC showed negligible toxicity describing their highly safe nature which can be attributed to the highly safe nature of exposed cyclodextrins. $_{BSA}$AgNPs showed slight safe profile than naked AgNPs and that can be explained as a result of masking of the highly reactive silver colloid surface. A coating of biological amphoteric molecule probably had decreased the adverse effect of silver colloids on challenged

cell membrane. Also BSA conjugation resulted in an increased molecular weight of the nanosystem resulting in the compromised cell membrane permeation, which further limited the intracellular cell death mechanisms. Finally the CβC-$_{BSA}$AgNPs toxicity profile clearly indicated the additive safety effects of surface linked CβC moieties, providing this nanoconjugate a much safer profile than AgNPs and $_{BSA}$AgNPs.

Table-1 Cytotoxic concentration, as determined by measuring the cell viability with the colorimetric formazan-based MTS assay.

Cell Line/ Sample	HeLa		HEL		VERO		MDCK	
	MCC	CC_{50}	MCC	CC_{50}	MCC	CC_{50}	MCC	CC_{50}
	µg/ml							
AgNPs	6.3± 0.7	431.7± 4.1	4.9± 1.2	396.2± 5.7	5.5± 0.3	403.5± 2.5	6.8± 0.8	465.2± 7.5
$_{BSA}$AgNPs	11.2± 1.5	620.8± 12.5	16.9± 2.2	528.2± 2.3	8.5± 1.2	603.5± 5.8	13.4± 1.7	703.8± 4.6
CβC	>100	>1000	>100	>1000	>100	>1000	>100	>1000
CβC-$_{BSA}$AgNPs	21.2±0.8	770.5± 2.5	18.2± 1.6	714.3± 6.4	14.7± 0.9	843.4± 1.6	24.2± 2.0	782.4± 5.2

3.6 Antifungal susceptibility testing

Serial dilution antifungal assays revealed the hybrid nature of synthesised nanobioconjugate "CβC-$_{BSA}$AgNPs". MIC and CC_{50} of all the challenged treatments in both the resistant and non-resistant strains are provided in **table-2**. It is very clear from this experiment that plain clotrimazole was displaying more than three times MIC and CC_{50} values in both the resistant *C albicans and C tropicalis* cells. Following these results, CβC also showed an elevated MIC and CC_{50} values in these clotrimazole resistant strains, but this increase is not of same potential as

seen with plain clotrimazole. The only reason responsible for this can be explained by the fact of controlled clotrimazole release from the dextrin cavity which is already mentioned in the CβC complex in-vitro release evaluation part.

Further the potential antifungal activity of AgNPs and $_{BSA}$AgNPs can be explained by their inherent nature to disrupt fungal cell membrane, produce ROS species and potential to cause intracellular damage. There was a noticeable difference between the *in-vitro* antifungal profile of naked and BSA stabilized AgNPs. Interestingly $_{BSA}$AgNPs showed slightly higher MIC and IC_{50} values, which can be understood by the fact that protein corona on the surface of AgNPs controls the direct surface interaction of metal colloid and fungal cell membrane. Whereas nanobioconjugate "CβC-$_{BSA}$AgNPs" displayed a potent antifungal profile on both the resistant and non-resistant cells. With the MIC value ~ 4µg/ml, which was significantly lower than its individual components, a potentiation was observed. Hybrid nature of the nanobioconjugate can be explained by the multi-targets attained to inhibit the fungal cell growth as explained in hypothesis proposed in **figure-1**. There are reports explaining the potentiated activity of dextrin functionalized AgNPs, which also justifies this potentiation. Moreover the nanoconjugate provide a higher localized antifungal concentration at the around or inside the fungal cell which leads to increased destruction. Inhibition kinetic study as depicted in **figure-7** clearly explains the potential of CβC-$_{BSA}$AgNPs to provide a hybrid antifungal therapeutics. In both the non-resistant and resistant fungal strains the death inhibition kinetic pattern after CβC-$_{BSA}$AgNPs exposure was having maximum negative slope.

It is important to discuss the mechanism behind the potential of CβC-$_{BSA}$AgNPs against clotrimazole resistant strains. Well it is very clear that boosted effectiveness was observed with the conjugate of cylodextrin entrapped clotrimazole (CβC) and $_{BSA}$AgNPs. Much improved

response from the CβC part (within CβC-$_{BSA}$AgNPs) in case of clotrimazole resistant strains is the major question. This can be explained by the fact that presence of stabilized colloidal silver would definitely worked against the molecular fungal cell operations responsible for this azole resistance.

Table-2 Antifungal susceptibility testing, estimation of MIC and IC_{50} of all the challenged treatments in both the resistant and non-resistant strains

Challenge	C albicans		C tropicalis		C albicans (Resistant Cells)		C tropicalis (Resistant Cells)	
	MIC	IC_{50}	MIC	IC_{50}	MIC	IC_{50}	MIC	IC_{50}
Clotrimazole	6.3±0.2	88.3±2.1	7.1 ±0.4	112.5±1.4	21.3±0.2	275±3.5	19.3±1.8	364.0±0.7
AgNPs	24.6±1.7	186.7±4.6	21.3±0.9	177.4±2.3	27.2±0.8	198.2±1.7	26.1±1.6	184.7±1.2
CβC	31.8±0.9	456.5±5.3	37.5±1.4	589.2±3.5	45.3±1.7	690.4±2.6	42.4±0.6	658.7±4.5
$_{BSA}$AgNPs	27.9±2.1	218.3±2.5	26.3±1.7	191.4±0.3	29.9±1.3	218.2±3.7	29.2±0.4	203.5±2.7
CβC-$_{BSA}$AgNPs	4.1±0.3	64.8±0.4	3.9±0.5	71.4±2.6	5.3±0.1	93.7±2.5	5.0±0.3	109.8±3.8

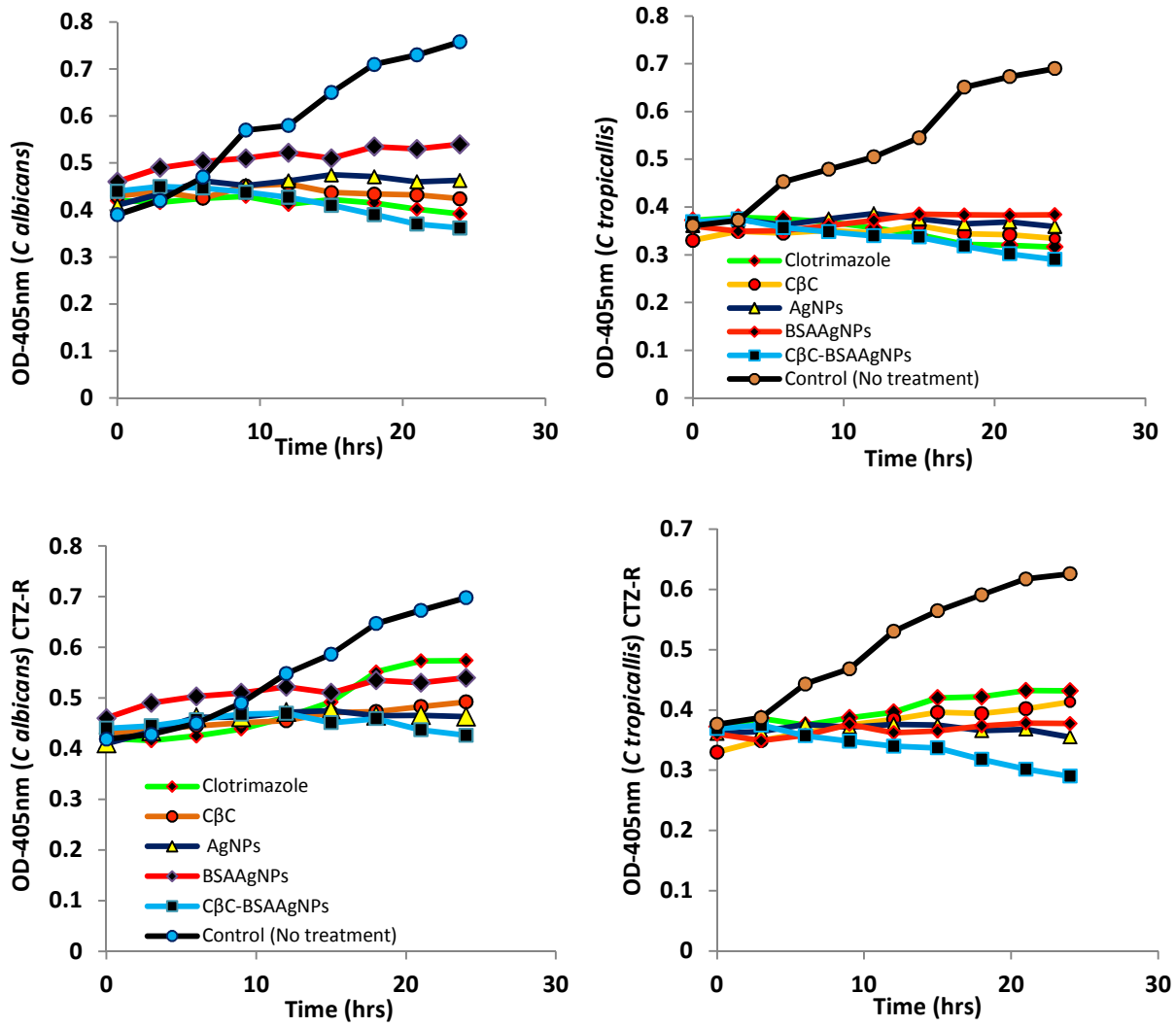

Figure-7 Inhibition kinetics after the exposure of IC_{50} concentrations of clotrimazole, CβC, AgNPs, $_{BSA}$AgNPs and CβC-$_{BSA}$AgNPs against both non-resistant and clotrimazole resistant fungal cells.

3.7 Apoptotic changes (Annexin V–propidium iodide double staining)

Study revealed the mechanistic comparison in the fungal cell inhibition after treatment with clotrimazole, CβC, AgNPs, $_{BSA}$AgNPs and CβC-$_{BSA}$AgNPs (**Figure-8**). Clotrimazole treatment

showed a sharp reduction in gated apoptotic cells in both the resistant cells, but this difference is not observed with CβC treatment. AgNPs and $_{BSA}$AgNPs both showed a comparatively high percentage of early apoptotic cells and it was very clear that no such discrimination is seen between resistant and non-resistant cells. Early apoptosis observed with the treatment of synthesised nanobiocomposite was uppermost and again the effect was unanimous in both resistant and non-resistant cells. Generation and accumulation of intracellular ROS is the possible reason behind the significantly higher apoptotic induction observed with nanosilver and AgNP based nanobiocomposite (34, 35).

3.8 ROS production

Production of ROS species due to the metabolism of cellular oxygen has been associated in the regulation of the apoptosis in fungal cells. Apoptosis study results made a strong mark for the involvement of the ROS species and this study confirms it on quantitative basis (as shown in **figure-9**). Minor level of ROS generation was observed in clotrimazole and CβC treated non-resistant cells, and these levels further fall down (comparative to control) in resistant cells. Treatment with naked AgNPs and $_{BSA}$AgNPs showed significantly higher level of ROS accumulation with similar quantitative values in both resistant and non-resistant cells. ROS accumulation in CβC-$_{BSA}$AgNPs treated cells is marginally higher when compared to AgNPs and $_{BSA}$AgNPs treated cells. Complying with the earlier antifungal and apoptotic effects results, it is very clear that AgNPs, $_{BSA}$AgNPs and CβC-$_{BSA}$AgNPs did not discriminated the clotrimazole resistance cells. ROS accumulation could be one of the major cell death mechanism involved in fungal cell inhibition, but these results again cleared the effectiveness of synthesised

nanobiocomposite and the simultaneous failure of fungal resistance machinery to work against the inhibition process of CβC-$_{BSA}$AgNPs.

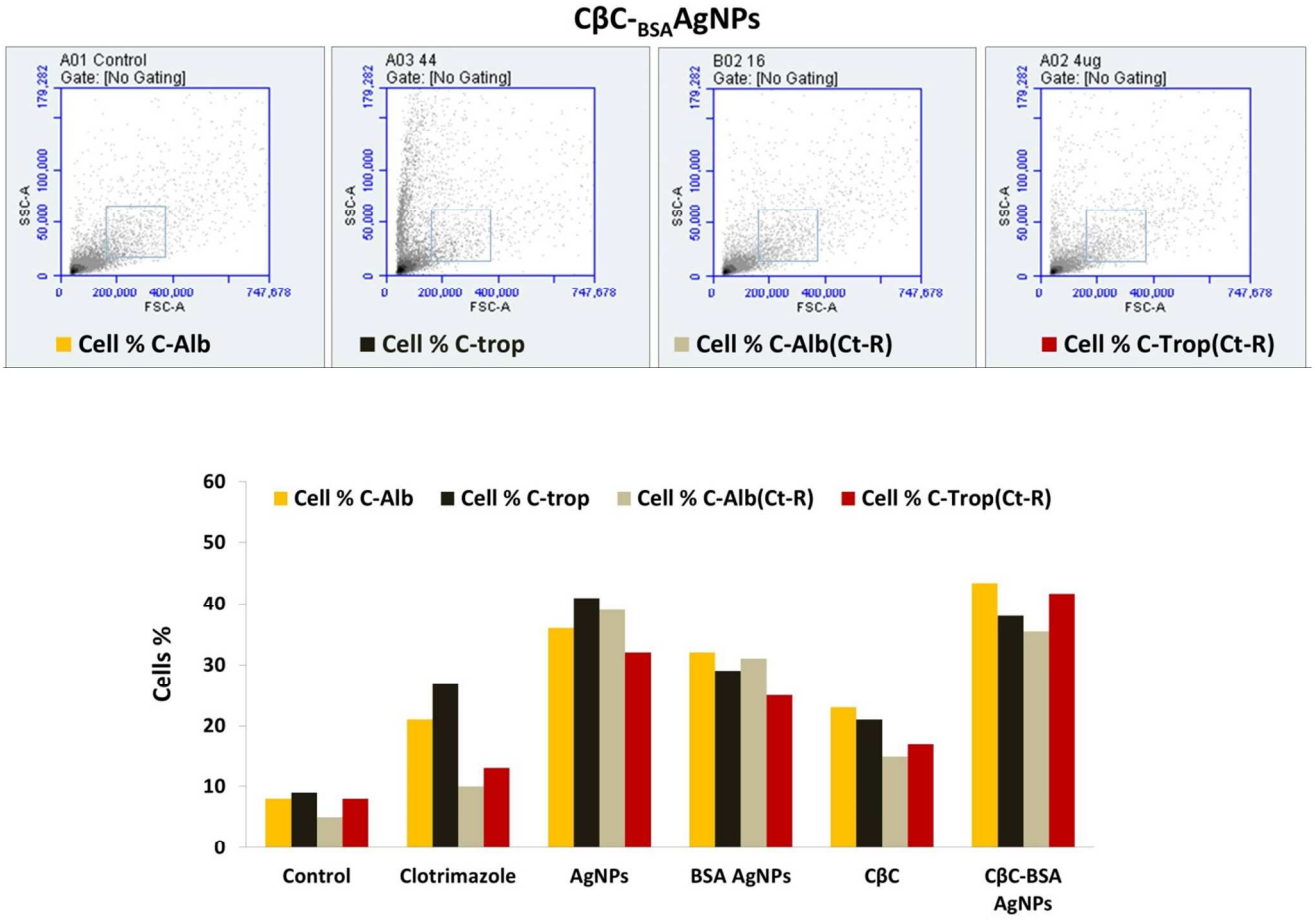

Figure-8 Apoptotic effect quantified by Annexin V–propidium iodide double staining procedure

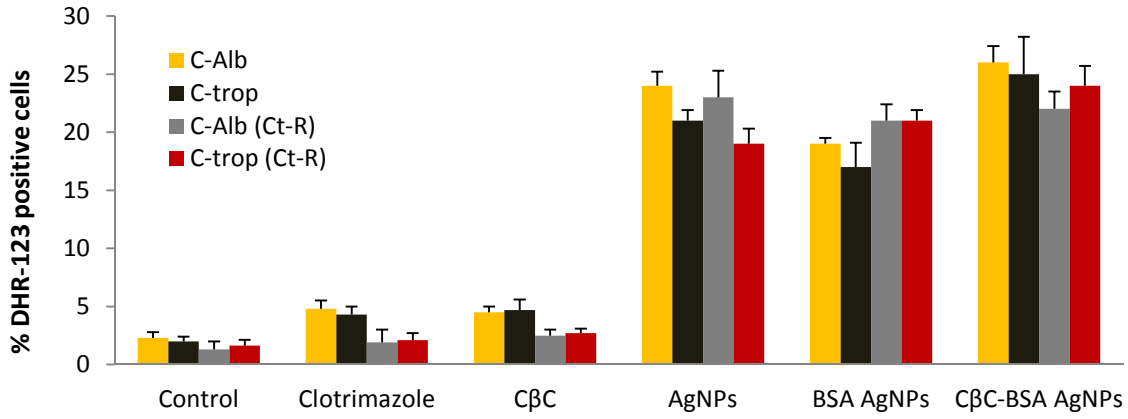

Figure-9 Quantitative ROS generation estimated by dihydrorhodamine 123 (DHR-123) positive fungal cells.

3.9 Cell cycle arrest after CβC-$_{BSA}$AgNPs treatment

Major percentage of treated cells was associated with G_2/M phase cell cycle arrest in all the treated fungal strains. As shown in **figure-10**, there was a significant elevation in the cell percentage detected in G_2/M phase, reflecting that treated cells were not able to enter the normal mitosis phase. Conversely a significant decrease in cells percentage observed in G_1 phase revealed a certain incapability of cellular machinery to enter into DNA synthesis and replication phase. So a general possibility of compromised fungal cell membrane and simultaneous disturbance of normal DNA synthesis process can be drafted due to the additive inhibitory effect of nanosilver and available clotrimazole moiety from **CβC-$_{BSA}$AgNPs.**

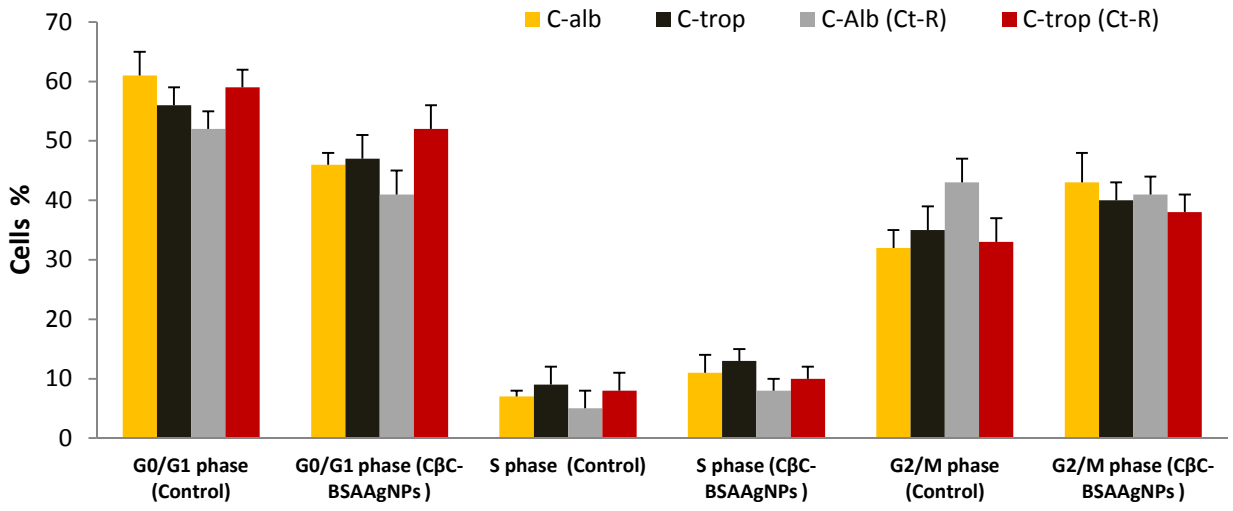

Figure-10 Effect of CβC-$_{BSA}$AgNPs on the cell cycle process of non-resistant and clotrimazole resistant fungal cells treated with its IC_{50} concentration.

CONCLUSION

Synthesised hybrid nanocomposite CβC-$_{BSA}$AgNPs was successfully synthesised using EDC/NHS chemistry, and characterization reports confirmed it. In-vitro release studies revealed a controlled and pseudo-first order release pattern of clotrimazole moiety and Ag ions. Cell cytotoxicity assay of different cell lines provided a comparatively safe profile when compared to naked and $_{BSA}$AgNPS. On challenging this biomacromolecule with stabilized silver core and surface attached pockets of clotrimazole against candida cells (both normal and clotrimazole resistant) a much improved and possible additive effect was seen. Mechanistic evaluation further revealed that early apoptosis due to frequent ROS generation in case of CβC-$_{BSA}$AgNPs treatment could be the possible reason. Undifferentiated inhibition in both clotrimazole resistant and normal fungal cells was solely reliant on the multiple inhibitory mechanisms possessed by nanosilver and the controlled release of the clotrimazole from the dextrin pockets at the target

site. Cell cycle analysis further confirmed the potential of the nanobioconjugate to interrupt with the normal cellular process such as mitosis and DNA replication. The work aimed at designing a nanosized biomacromolecule with improved antifungal activity on even resistant cells. The scope of this strategy can be well exploited where limited choice of therapeutics and the problem of resistance are overlapped. Moreover, use of a nanometal core/base provides a dual benefit of both inherent therapeutic potential and nanobase to develop a functionalized hybrid biomacromolecule.

ACKNOWLEDGEMENT

Author acknowledges Department of Biotecthnology (DBT) India, Punjab Technical University, Jalandhar, Punjab State Council of Science and Technology (PSCST) India, Department of Virology, Haffkine Institute for Training Research and Testing, Parel, Mumbai, India for providing the supportive facility and financial base for this research. Author also acknowledges the insightful discussions provided by Dr Jitender Bhariwal (Department of Medicinal Chemistry, ISF-CP, Moga, Punjab, India) and technical support from Prof. R. Snoeck and Prof. G. Andrei (Laboratory of Virology and Chemotherapy, Department of Microbiology and Immunology, Rega Institute, Belgium.

REFERENCE

1. Mazel D, Davies J. Antibiotic resistance in microbes. Cellular and Molecular Life Sciences CMLS. 1999;56(9-10):742-54.
2. Walsh C. Antibiotics: actions, origins, resistance: American Society for Microbiology (ASM); 2003.
3. Gottesman MM. Mechanisms of cancer drug resistance. Annual review of medicine. 2002;53(1):615-27.
4. Davies J, Davies D. Origins and evolution of antibiotic resistance. Microbiology and Molecular Biology Reviews. 2010;74(3):417-33.
5. Lupetti A, Danesi R, Campa M, Del Tacca M, Kelly S. Molecular basis of resistance to azole antifungals. Trends in molecular medicine. 2002;8(2):76-81.
6. Ryley JF, Wilson RG, Barrett-Bee KJ. Azole resistance in Candida albicans. Sabouraudia. 1984;22(1):53-63.
7. Canuto MM, Rodero FG. Antifungal drug resistance to azoles and polyenes. The Lancet infectious diseases. 2002;2(9):550-63.
8. Johnson EM, Warnock DW, Luker J, Porter SR, Scully C. Emergence of azole drug resistance in Candida species from HIV-infected patients receivingprolonged fluconazole therapy for oral candidosis. Journal of Antimicrobial Chemotherapy. 1995;35(1):103-14.
9. White TC. Increased mRNA levels of ERG16, CDR, and MDR1 correlate with increases in azole resistance in Candida albicans isolates from a patient infected with human immunodeficiency virus. Antimicrobial Agents and Chemotherapy. 1997;41(7):1482-7.
10. Masitas RA, Khachian IV, Bill BL, Zamborini FP. Effect of Surface Charge and Electrode Material on the Size-Dependent Oxidation of Surface-Attached Metal Nanoparticles. Langmuir. 2014;30(43):13075-84.
11. Viñes F, Gomes JR, Illas F. Understanding the reactivity of metallic nanoparticles: beyond the extended surface model for catalysis. Chemical Society Reviews. 2014;43(14):4922-39.
12. Jain J, Arora S, Rajwade JM, Omray P, Khandelwal S, Paknikar KM. Silver nanoparticles in therapeutics: development of an antimicrobial gel formulation for topical use. Molecular Pharmaceutics. 2009;6(5):1388-401.
13. Fedlheim DL, Foss CA. Metal nanoparticles: synthesis, characterization, and applications: CRC Press; 2001.
14. Panáček A, Kolář M, Večeřová R, Prucek R, Soukupová J, Kryštof V, et al. Antifungal activity of silver nanoparticles against Candida spp. Biomaterials. 2009;30(31):6333-40.
15. Jain PK, Huang X, El-Sayed IH, El-Sayed MA. Noble metals on the nanoscale: optical and photothermal properties and some applications in imaging, sensing, biology, and medicine. Accounts of Chemical Research. 2008;41(12):1578-86.
16. Kim K-J, Sung WS, Suh BK, Moon S-K, Choi J-S, Kim JG, et al. Antifungal activity and mode of action of silver nano-particles on Candida albicans. Biometals. 2009;22(2):235-42.
17. Monteiro D, Gorup L, Silva S, Negri M, de Camargo E, Oliveira R, et al. Silver colloidal nanoparticles: antifungal effect against adhered cells and biofilms of Candida albicans and Candida glabrata. Biofouling. 2011;27(7):711-9.
18. Sardi J, Scorzoni L, Bernardi T, Fusco-Almeida A, Giannini MM. Candida species: current epidemiology, pathogenicity, biofilm formation, natural antifungal products and new therapeutic options. Journal of medical microbiology. 2013;62(Pt 1):10-24.
19. Loeffler J, Stevens DA. Antifungal drug resistance. Clinical Infectious Diseases. 2003;36(Supplement 1):S31-S41.

20. Pelletier R, Peter J, Antin C, Gonzalez C, Wood L, Walsh TJ. Emergence of resistance of Candida albicans to clotrimazole in human immunodeficiency virus-infected children: in vitro and clinical correlations. Journal of clinical microbiology. 2000;38(4):1563-8.
21. Odds FC, Brown AJ, Gow NA. Antifungal agents: mechanisms of action. Trends in microbiology. 2003;11(6):272-9.
22. El-Nour KMA, Eftaiha Aa, Al-Warthan A, Ammar RA. Synthesis and applications of silver nanoparticles. Arabian journal of chemistry. 2010;3(3):135-40.
23. Murawala P, Phadnis S, Bhonde R, Prasad B. In situ synthesis of water dispersible bovine serum albumin capped gold and silver nanoparticles and their cytocompatibility studies. Colloids and Surfaces B: Biointerfaces. 2009;73(2):224-8.
24. Dominguez-Medina S, Blankenburg J, Olson J, Landes CF, Link S. Adsorption of a protein monolayer via hydrophobic interactions prevents nanoparticle aggregation under harsh environmental conditions. ACS sustainable chemistry & engineering. 2013;1(7):833-42.
25. Gaurav C, Goutam R, Rohan KN, Sweta KT, Abhay CS, Amit GK. (Copper–curcumin) β-cyclodextrin vaginal gel: Delivering a novel metal–herbal approach for the development of topical contraception prophylaxis. European Journal of Pharmaceutical Sciences. 2014;65:183-91.
26. Fischer MJ. Amine coupling through EDC/NHS: a practical approach. Surface plasmon resonance: Springer; 2010. p. 55-73.
27. Malich G, Markovic B, Winder C. The sensitivity and specificity of the MTS tetrazolium assay for detecting the in vitro cytotoxicity of 20 chemicals using human cell lines. Toxicology. 1997;124(3):179-92.
28. Caviglia C, Zor K, Montini L, Tilli V, Canepa S, Melander F, et al. Impedimetric toxicity assay in microfluidics using free and liposome-encapsulated anticancer drugs. Analytical chemistry. 2015;87(4):2204-12.
29. Dal Pozzo F, Andrei G, Daelemans D, Winkler M, Piette J, De Clercq E, et al. Fluorescence-based antiviral assay for the evaluation of compounds against vaccinia virus, varicella zoster virus and human cytomegalovirus. Journal of virological methods. 2008;151(1):66-73.
30. Castilho AL, Caleffi-Ferracioli KR, Canezin PH, Siqueira VLD, de Lima Scodro RB, Cardoso RF. Detection of drug susceptibility in rapidly growing mycobacteria by resazurin broth microdilution assay. Journal of microbiological methods. 2015;111:119-21.
31. Martin MN, Allen AJ, MacCuspie RI, Hackley VA. Dissolution, Agglomerate Morphology, and Stability Limits of Protein-Coated Silver Nanoparticles. Langmuir. 2014;30(38):11442-52.
32. Kittler S, Greulich C, Diendorf J, Koller M, Epple M. Toxicity of silver nanoparticles increases during storage because of slow dissolution under release of silver ions. Chemistry of Materials. 2010;22(16):4548-54.
33. Benn TM, Westerhoff P. Nanoparticle silver released into water from commercially available sock fabrics. Environmental science & technology. 2008;42(11):4133-9.
34. Dixon SJ, Stockwell BR. The role of iron and reactive oxygen species in cell death. Nature chemical biology. 2014;10(1):9-17.
35. Avery SV. Oxidative Stress and Cell Function. Systems Biology of Free Radicals and Antioxidants. 2014:89-112.